Ternary Fe-Cu-Ni many-body potential to model reactor pressure vessel steels: First validation by simulated thermal annealing — Source link ↗

Giovanni Bonny, Roberto C Pasianot, Nicolas Castin, Lorenzo Malerba

Institutions: Ghent University, National Scientific and Technical Research Council, Université libre de Bruxelles

Topics: Reactor pressure vessel and Interatomic potential

Related papers:

- Fast parallel algorithms for short-range molecular dynamics

- Development of new interatomic potentials appropriate for crystalline and liquid iron

- Structural stability and lattice defects in copper: Ab initio , tight-binding, and embedded-atom calculations

- Visualization and analysis of atomistic simulation data with OVITO–the Open Visualization Tool

- Embedded-atom method: Derivation and application to impurities, surfaces, and other defects in metals

Ternary Fe-Cu-Ni many-body potential to model reactor pressure vessel steels: First validation by simulated thermal annealing

Giovanni Bonny, Roberto C Pasianot, Nicolas Castin, Lorenzo Malerba

Ternary Fe-Cu-Ni many-body potential to model reactor pressure vessel steels: First validation by simulated thermal annealing

Ternary Fe-Cu-Ni many-body potential to model reactor pressure vessel steels: First validation by simulated thermal annealing

G. Bonny[1,2,*], R.C. Pasianot[3,4,5], N. Castin[1,6] and L. Malerba[1]

[1] SCK•CEN, Nuclear Materials Science Institute, Boeretang 200, B-2400 Mol, Belgium

[2] Ghent University, Center for Molecular Modeling, Proeftuinstraat 86, B-9000 Gent, Belgium

[3] CAC-CNEA, Departamento de Materiales, Avda. Gral. Paz 1499, 1650 San Martín, Argentina

[4] CONICET, Avda. Rivadavia 1917, 1033 Buenos Aires, Argentina

[5] Instituto Sábato, UNSAM/CNEA, Avda. Gral. Paz 1499, 1650 San Martín, Argentina

[6] Université Libre de Bruxelles (ULB), Physique des Solides Irradiés et des Nanostructures (PSIN), Bd. du Triomphe CP234, 1050 Brussels, Belgium.

Abstract

In recent years the development of atomistic models dealing with microstructure evolution and subsequent mechanical property change in reactor pressure vessel steels has been recognised as an important complement to experiments. In this framework, a literature study has shown the necessity of many-body interatomic potentials for multi-component alloys. In this paper we develop a ternary many-body Fe-Cu-Ni potential for this purpose. As a first validation, we used it to perform a simulated thermal annealing study of the Fe-Cu and Fe-Cu-Ni alloys. Good qualitative agreement with experiments is found, although fully quantitative comparison proved impossible, due to limitations in the used simulation techniques. These limitations are also briefly discussed here.

1. Introduction

In recent years the development of models tracing the microstructure evolution and subsequent mechanical property change in reactor pressure vessel (RPV) steels, employing a computer-based multi-scale approach, has been recognised as an important complement to

---
[*] Corresponding author, email: gbonny@sckcen.be

experiments, in support of the surveillance programmes of existing nuclear power plants (NPPs) [1]. The development of physical models of this type is considered particularly important in view of the extension of the service lifetime of NPPs, as for this purpose the available database from surveillance specimens is not sufficient and solid models suitable to be extrapolated are therefore required in order to prove the capability of the materials to perform their duty for a time twice as long than foreseen.

RPV steels used in Western-type light water reactor NPPs are low-alloyed bainitic steels, containing as main alloying elements nickel, manganese and often molybdenum, as well as consistent traces of silicon, copper and, to a lesser extent, chromium, sulphur and phosphorus. The low solubility of copper in iron leads to radiation-enhanced formation of ultrafine copper-rich precipitates during operation at 290°C, which atom probe studies have revealed to contain nickel, manganese, silicon, and sometimes phosphorus as well [2-4]. Even in low-copper steels, precipitates rich in manganese and nickel are detected, while phosphorus atoms have in all cases the tendency to distribute in a heterogeneous manner, associated or not with other precipitates [4-6]. The formation of these different types of precipitates may be at least partly radiation-induced, but no consensus exists about their actual origin, nature and mechanism of formation. There is, however, consensus about the fact that the interaction of these nano-defects with dislocations is the main cause of hardening and embrittlement of these steels [7-16]. In this framework, large scale atomistic simulations in multi-component alloys are of fundamental importance with a view to cast some light on the mechanisms leading to the formation of the mentioned different classes of precipitates, as well as in order to study in detail their interaction with dislocations as source of hardening.

In the literature a few works studying precipitation in multi-component alloys representing RPV steels exist. For example, in the works of Liu *et al.* [17] and Odette and Wirth [18], precipitation in the Fe-Cu-Ni-Mn-Si model alloy is studied by means of rigid lattice exchange Monte Carlo (MC). Therein the atomic interactions were parameterized by approximate pair bond potentials derived from thermodynamic data. However, simple pair potentials are inadequate to treat diffusion and cannot correctly describe defect configurations (see [19, 20] and references therein). Therefore they are inadequate to trace the micro-structural evolution of the alloy in real time and offer limited transferability to off-lattice atomistic methods, for example molecular dynamics (MD). Other works include the ones by Vincent *et al.* [21, 22], where rigid lattice kinetic MC was performed on the same model alloy. In those works the interatomic interactions were parameterized by pair interactions based on density functional theory (DFT) calculations. Also here the interatomic interactions

are not transferrable to off-lattice approaches, thereby limiting the applicability of the model. From these works it is clear that more realistic and extendable simulations (including off-lattice approaches, allowing for example also dislocation-precipitate interaction studies) require the development of reliable multi-component many-body interatomic potentials.

In this framework we present a many-body interatomic potential for a ternary alloy, namely Fe-Cu-Ni, developed in such a way that both the alloy's thermodynamic properties and the interaction between solute atoms and point-defects is properly reproduced, as compared to, respectively, the experimental phase diagram and density functional theory (DFT) calculations. The choice of the Fe-Cu-Ni alloy as first step towards the development of potentials for multi-component systems was dictated by the fact that these two alloying elements are phenomenologically considered to be the main responsibles for RPV steel hardening and embrittlement [13, 23].

As a first validation of our potential, we carried out an atomistic study regarding precipitation in Fe-Cu and Fe-Cu-Ni alloys, to determine the effect of Ni on Cu precipitate formation. For this purpose, we used molecular static (MS) calculations to characterize Cu-precipitate/Ni interaction and atomistic kinetic Monte Carlo (AKMC) to trace the micro-chemical evolutions of the alloy.

2. Methodology

Energy formalism

The atomic interactions are described using the embedded atom method (EAM) [24], which is widely used to describe metals and their alloys. In addition to pair interactions, V, this approach includes an embedding energy, F, dependent on the local electron density, ρ. The latter contribution approximates the many-body contribution of all nearby atoms. The total energy within EAM is given as,

$$E = \frac{1}{2} \sum_{\substack{i,j=1 \\ j \neq i}}^{N} V_{t_i t_j}(r_{ij}) + \sum_{i=1}^{N} F_{t_i}(r_i).$$ (1)

Here N represents the total number of atoms in the system, r_{ij} is the distance between atoms i and j, and t_i denotes the atom-type (Fe, Cu or Ni in our case). The local electron density around atom i, contributed from its neighbours is given as,

$$r_i = \mathop{\mathring{a}}_{\substack{j=1 \\ j^1 i}}^{N} j_{t_j}(r_{ij}),$$

(2)

where ρ denotes the electron density function of the considered element. Thus, for the Fe-Cu-Ni ternary system twelve functions need to be defined: φ_{Fe}, φ_{Cu}, φ_{Ni}, F_{Fe}, F_{Cu}, F_{Ni}, V_{FeFe}, V_{CuCu}, V_{NiNi}, V_{FeCu}, V_{FeNi} and V_{CuNi}.

The pure species functions are taken from the literature, choosing the most suitable among those currently available. For Fe we choose 'potential 2' developed by Mendelev *et al.* [25], for Cu we choose 'EAM 1' developed by Mishin *et al.* [26] and for Ni we adopted the potential developed by Voter and Chen [27]. Within EAM, however, the forms of V, F and φ are not uniquely determined. Two transformations [19, 28, 29], $\hat{T}_1$ and $\hat{T}_2$, exist that leave the total energy invariant,

$$\hat{T}_1 \begin{cases} j(r) \circledR Sj(r) \\ F(r) \circledR F(r/S) \end{cases}$$

(3)

$$\hat{T}_2 \begin{cases} F(r) \circledR F(r) + Cr \\ V(r) \circledR V(r) - 2Cj(r) \end{cases},$$

(4)

with C and S arbitrary constants. Therefore the units of the electron density are arbitrary for the pure species, but contribute to each others' embedding energy in the alloy case. To assure *a priori* an equal contribution to the electron density from all elements, we use transformations $\hat{T}_1$ and $\hat{T}_2$ with $C=-F'(\rho_{eq})$ and $S=1/\rho_{eq}$ to transform the pure potentials to their "effective gauge" form [19], where $F'(\rho_{eq})=0$ and $\rho_{eq}=1$ on the bcc equilibrium lattice.

Following this, the three cross interactions V_{FeCu}, V_{FeNi} and V_{CuNi} and the relative weight between the electron densities ρ_{Fe}/ρ_{Cu}, ρ_{Fe}/ρ_{Ni} need to be determined. The cross pair potentials V_{FeCu}, V_{FeNi} and relative weights between the electron densities ρ_{Fe}/ρ_{Cu}, ρ_{Fe}/ρ_{Ni} are taken from the works by Pasianot and Malerba [30] and Bonny *et al.* [31], respectively. Therefore, our fitting effort is focussed on V_{CuNi}. In all cases the cross pair potentials are parameterized by the cubic spline expansion,

$$V(r_{ij}) = \sum_{k=1}^{N_p} a_k (r_k - r)^3 H(r_k - r), \qquad (5)$$

where N_p denotes the number of knots, a_k are the fitting parameters and H denotes the Heaviside unit step function.

Interatomic potential fitting strategy

For the study of radiation damage production and evolution, a potential must reproduce the alloy's thermodynamics, kinetics and defect interactions reasonably well. The kinetics of the alloy transformation is largely defined by point-defect migration barriers for particular configurations of solute atoms around the defect in the host matrix. The defect interactions are characterized by the binding energies between solute complexes and solute point-defect complexes.

The Fe potential used in this work has been widely used, tested and has demonstrated so far to be the one that succeeds at best in reproducing the properties of iron that are of interest for radiation damage studies [32], including dislocation properties [33]. The Cu and Ni potentials, though not specifically developed to model radiation damage, represent state-of-the-art potentials that are suitable for our purposes. The Fe-Cu and Fe-Ni interactions were fitted using the experimental phase diagram as direct reference, while using DFT indications to fit the point-defect/solute-atom interaction and vacancy migration barriers, as described in [30, 31, 34].

The Cu-Ni interaction is here fitted to a Calphad parameterized mixing enthalpy [35]. Since the Cu-Ni system consists of a simple miscibility gap of two fcc phases [35-38], a fit to the randomly disordered mixing enthalpy proved sufficient for a reasonable reproduction of the Calphad parameterized miscibility gap [34]. Information about point defects was included by fitting to the interaction energy of Ni-Cu pairs and the Ni-Cu $\langle 110 \rangle$ dumbbell, all obtained via DFT calculations in the bcc Fe matrix [21-22]. Note that no defect properties were fitted in the fcc Ni-Cu binary alloy and their proper description can therefore *a priori* not be guaranteed. Taking into account the above described thermodynamic properties for the Cu-Ni binary and defect interactions in the Fe-Cu-Ni ternary, the spline coefficients in Eq. (5) are optimized. The parameters for all cross potentials are given in Appendix A.

Atomistic kinetic Monte Carlo simulations

The thermal annealing of binary Fe-Cu and ternary Fe-Cu-Ni alloys was modelled using a rigid lattice AKMC technique [39]. Initially, the Cu and Ni atoms are randomly distributed in a bcc Fe matrix. The evolution of the system leading to the atomic redistribution is driven by single vacancy diffusion. The diffusion jump frequency of the vacancy, Γ, is evaluated as a thermally activated process,

$$G = n_0 \exp(-E_m / k_B T) , \qquad (6)$$

where ν_0 is an attempt frequency chosen to be constant and equal to 6×10^{12} s^{-1}, E_m is the local atomic environment (LAE)-dependent migration energy, k_B is Boltzmann's constant and T is the absolute temperature. Note that *a priori* the attempt frequency ν_0 is both temperature and LAE-dependent through magnetic and vibrational entropy; however, variations of Γ due to the LAE-dependence of E_m are numerically of significantly more importance [40]. Thus, a proper estimation of E_m is essential for a correct description of the micro-chemical evolution of the alloy.

In the literature, many approximations to describe E_m in terms of the LAE exist; for example, the Kang-Weinberg decomposition [41] based on total energy differences and broken-bond counting [42]. However, as shown in [40, 43], E_m estimated in such a way may be very approximate as compared to a proper barrier estimation, for example by using drag [44] or nudged elastic band (NEB) methods [45]. Recently, a regression method based on artificial neural networks (ANNs) was developed that closely reproduces NEB obtained values of E_m at the same computational cost as the Kang-Weinberg decomposition [43, 46, 47]. In this work, the latter method was chosen and applied to compute E_m during the AKMC simulations.

In short, the method works as follows. First, an adequate amount ($\sim 10^5$) of NEB-obtained migration barriers, calculated with our potential, is produced, for randomly chosen LAE configurations. The obtained values inherently include 0 K relaxation effects. Thus, a database of migration barrier examples is built: 40% is used for the training of the ANN, while ~60% is used for the validation of the ANN predicted values. This strategy provided an ANN optimised to predict E_m for LAEs encountered during simulated thermal annealing. More details on the applied method are provided in [43, 46, 47].

In a bcc lattice, there are eight possible first nearest neighbour sites whereto a single vacancy can jump (exchanges with farther neighbours require much higher migration energies). In the model adopted here, each vacancy jump corresponds to a Monte Carlo step. The jump to be performed is chosen based on its probability, evaluated in terms of jump frequency. The time between two jumps is calculated according to a mean residence time algorithm, i.e. the inverse of the sum of the eight possible jump frequencies [39].

Finally, for the purpose of validating our potential, we performed AKMC simulations on the Fe-1.13Cu and Fe-1.13Cu-1.36Ni alloys at 823 K, for which experimental data are available in the literature [48]. The AKMC simulations were performed in cubic boxes containing 128,000 atoms until coarsening regime was reached, which amounts to a MC time, t_{MC}, of ~0.3 s. As further discussed in Section 4, the MC time in a thermal ageing simulation cannot be directly compared to real time: the corresponding real time is much longer and to estimate it an appropriate way time renormalization must be applied [49].

3. Results

Static properties

The binding energies (positive sign indicating attractive interaction) of the ternary defect complexes, calculated by molecular statics (MS) with our potential, are compared with the corresponding DFT values [21-22] in Table 1. The latter data suggest a negligible interaction between isolated Cu and Ni atoms in the bcc Fe matrix and the instability of the mixed $\langle 110 \rangle$ dumbbell, for both solutes. Both effects are reasonably well reproduced by our potential and suggest a reasonable defect behaviour description.

Regarding the thermodynamic behaviour of our potential, the mixing enthalpy obtained by MS in random alloys is compared to the most recent ones from the Calphad database [35, 38], in Fig. 1. Clearly, the agreement with the parameterization by Srikanth *et al.* (the target curve) is very good. The miscibility gap calculated with our potential is compared with the two existing ones built from the Calphad database [35, 38] in Fig. 2. The miscibility gap based on our potential was calculated using MC simulations in the semi-grand canonical (transmutation) ensemble, as explained in more detail in [34]. Given the limited degree of freedom for fitting (due to the already predetermined electronic density weights ρ_{Fe}/ρ_{Cu} and ρ_{Fe}/ρ_{Ni}), and the large variation in the miscibility gap built from the Calphad database, the agreement between potential and database can be considered reasonable.

Prior to the simulated thermal annealing, we performed static calculations to study the stability range of coherent Cu precipitates in the bcc Fe-matrix and its interaction with Ni. Firstly, pure coherent Cu precipitates of different sizes were relaxed by means of MS calculations. During the relaxation, the coordination number of the atoms inside the Cu precipitate was monitored to reveal possible crystallographic transformations. From these calculations it was found that Cu precipitates with a size up to 2.5 nm remain stable. Above this size, the precipitate tries to change its bulk crystal structure. Experimentally, Cu precipitates were observed to be coherent with the bcc Fe-matrix up to an average size of 4-5 nm, after which they transform into a 9R and eventually into a fcc structure [50-52]. We thus conclude that the stability range of coherent bcc Cu precipitates predicted by our potential is in the correct range, though perhaps somewhat underestimated.

Secondly, we performed MS calculations to examine the interaction between a Cu precipitate and a Ni atom in the bcc Fe-matrix. To do so, the binding energy between a Ni atom and a Cu precipitate (of size 1, 2 and 2.5 nm) was calculated as a function of the distance between the Ni atom and centre of the Cu precipitate. To increase statistics, the Ni atom was moved along different crystallographic directions ($\langle 100 \rangle$, $\langle 110 \rangle$, $\langle 111 \rangle$ and $\langle 112 \rangle$). The results of these calculations are presented in Fig. 3, where the abscissa is the distance from the Cu precipitate centre in reduced units (with R_p the precipitate radius). The figure clearly shows strong attractive interaction between the Ni atom and the surface of the Cu precipitate. This attractive interaction decreases fast with increasing distance between atom and precipitate. For a Ni atom inside the Cu precipitate, the interaction is always repulsive. The curves presented in Fig. 3 are in agreement with the experimental observations of Ni-enrichment at the surface of Cu precipitates [3, 4, 48]. In addition, it is important to note that the binding energy curves for the unrelaxed configurations are almost coincident with the binding energy curves for the relaxed configurations presented in Fig. 3. This observation suggests that the binding of Ni on a Cu precipitate surface is a chemical effect, rather than an effect due to the strain field around the (oversized) Cu precipitate. This finding partially justifies the application of a rigid lattice MC technique to simulate the thermal annealing of Fe-Cu-Ni alloys.

Simulated thermal ageing

Formatted: Bullets and Numbering

Visual inspection of the configurations obtained during the simulations show that for both studied alloys Cu-rich precipitates are formed. The Ni distribution in the ternary alloy appears

to remain random under the present thermal ageing conditions. From the analysis of the extracted configurations, the precipitate density, N_p, mean diameter, d_p, and solute concentration in the matrix, x_S, were computed as a function of t_{MC}. These results for both alloys are shown in Figs. 4, 5 and 6, respectively. From these figures, supported by visual inspection, the precipitation process appears to occur by the nucleation, growth and coarsening. The steep increase in N_p during the first fractions (~5 ms) of the simulation denotes the nucleation process. At the maximum density, N_p remains approximately constant and d_p steadily increases. This, combined with a steep decrease of x_{Cu} in the matrix, indicates a stage of dominant growth in the interval ~5-25 ms. Beyond 25 ms, N_p decreases with t_{MC} while d_p keeps increasing, which indicates the coarsening stage, where large precipitates grow at the cost of the dissolution or coalescence of smaller ones. However, the simultaneous decrease of x_{Cu}, even beyond 25 ms, indicates that the precipitation occurs by a mixture of growth and coarsening.

As already mentioned, the Ni atoms in the matrix remain randomly distributed during the whole simulation. At the nucleation stage, however, they act as nucleation centres for Cu precipitates. This clearly follows from Fig. 4, where the peak density for the Fe-Cu-Ni alloy is ~29% higher than for the Fe-Cu alloy. This is in agreement with experimental observations by Buswell *et al.* [48], where a density increase of ~34% was observed due to the addition of Ni. This observation is further supported by the observation that x_{Ni} in the matrix decreases during the nucleation stage and then immediately saturates to its equilibrium value. Since x_{Ni} remains constant during growth and coarsening stage, Ni does not migrate from the matrix to the Cu precipitate surface. Instead, the Ni enclosed in the Cu precipitates due to nucleation and growth is expelled to the precipitate surface. This is also consistent with the static calculations presented in Section 3.1, and rigid lattice MC simulations in the Refs. [17, 18, 21]. In Fig. 5, we also observe that d_p is lower, due to the addition of Ni, which is also in qualitative agreement with experimental observations by Buswell *et al.* [48]. Near the end of our simulation, however, both N_p and d_p, with and without Ni, converge to a common value, which is also observed in the latter experiment.

An example for a typical size distribution of the Cu-rich precipitates during the late growth/early coarsening is plotted in Fig. 7, which shows a multi-modal distribution of the precipitate size (each mode corresponds to a Cu-rich precipitate). With increasing t_{MC}, the mean size of the clusters increases (as shown in Fig. 4) and the maximum density in the first mode decreases (due to the depletion of the matrix and dissolution of small clusters). However, the distribution of small clusters (<10 atoms) remains non-zero during the whole

simulation. Past the nucleation stage, when no new clusters are nucleated, such small clusters are below the critical size for nucleation. Therefore, the maximum cluster size for which this distribution is non-zero gives an estimate for the critical cluster size for nucleation. Above this size, the nuclei are stable and spontaneously grow into Cu-rich precipitates, which are part of the second mode of the distribution. Following this logic, we estimate the critical cluster size to be ±5-8 atoms, which is well below the resolution of any experimental technique.

4. Discussion

Prior to discussing the AKMC results, we discuss the quality of the migration barriers estimated by our ANN. The quality of the agreement between the ANN predictions and NEB calculated barriers defines how good the ANN represents our potential. In Fig. 8 the barriers calculated using NEB and our potential are compared to the ANN predicted ones for the Fe-V, Cu-V and Ni-V exchanges for randomly chosen LAEs, as described in Section 2.3. From the data in the figure we calculated that the average error for Fe-V exchange is 3.7%, for Cu-V exchange it is 3.5% and for Ni-V exchange it is 4.3% . As a comparison, a more heuristic estimation of E_m, for example by the Kang-Weinberg decomposition [40], provides average errors amounting to 52.0% . Therefore we believe that, at present, the ANN provides the best compromise between accuracy and computation time to estimate the LAE dependent E_m. A more detailed discussion on this subject can be found in Refs [43, 47].

In our AKMC simulations, the vacancy concentration is $1/N$ and is imposed by the box size, N being the number of atoms in the box. This concentration is typically a large overestimation of the physical equilibrium vacancy concentration in an alloy. To account for this, t_{MC} must be rescaled to obtain the real physical annealing time, t_{real}. Here, we use a method described in Refs. [41, 53] and briefly describe the procedure below. During the simulations, the vacancy concentration in the matrix, $C_V^{MC}(M)$, defined as the concentration on sites without Cu atoms among their first and second nearest neighbours, is computed as,

$$C_V^{MC}(M) = \frac{f_V^M}{N\,X_M}\,.$$

(7)

Here f_V^M is the fraction of time spent by the vacancy in the matrix and X_M is the atomic fraction of the matrix main element ($X_M \approx 1$ in dilute alloys as those considered here). The true vacancy equilibrium concentration in the matrix material, $C_V^{eq}(M)$, is given as,

$$C_V^{eq}(M) = \exp(-E_f^V / k_B T),$$ (8)

E_f^V being the formation energy of a vacancy in the matrix, thereby neglecting the entropic contributions. As a result, t_{real} is related to t_{MC} via the equation,

$$t_{real} = t_{MC} \frac{C_V^{MC}(M)}{C_V^{eq}(M)}.$$ (9)

This scheme of time renormalization guarantees a diffusion coefficient of the solutes in the matrix that remains constant during the precipitation process. Following this procedure, we find a conversion factor of ~23 for the Fe-Cu binary alloy, where we took $E_f^V = 1.71$ eV and $f_V^M = 10^{-4}$ as calculated in our simulations. The maximum obtained t_{MC}, on the other hand, is of the order of 1 s; therefore the maximum t_{real} obtained in our simulations is of the order of 23 s. This time is at least an order of magnitude shorter than typical (short) experimental annealing times that are of the order of hours. Therefore, direct quantitative comparison with thermal ageing experiments is impossible and only a qualitative comparison was presented above.

The short physical annealing time is also the reason for small precipitate size, $d_p \sim 1$ nm, and large precipitate density, $N_p \sim 10^{25}$ m^{-3}, obtained during our simulations. In experiments, typical values for precipitate size and density are $d_p \sim 4$ nm and $N_p \sim 10^{23}$ m^{-3}, respectively, for an ageing time of 2 h at the same temperature as our simulations [48]. Furthermore, the limited box size used for our simulations is also a restrictive factor. If we assume that all the Cu in our simulation box forms one spherical precipitate, its size would be 3.2 nm at most and the corresponding density would be 6.7×10^{23} m^{-3}, which gives an upper and lower limit for d_p and N_p, respectively. For a proper comparison to experiments, we should thus also increase the simulation box by at least an order of magnitude. Noting that the physical simulation time shows a quadratic increase with box size [54], it is clear that our AKMC tool in its current implementation is not adequate for direct comparison with experiments.

To achieve the latter, the AKMC method must be accelerated by a few orders of magnitude. Because in our simulations the vacancy is trapped inside the precipitate by more than 99% of the computation time ($f_V^M = 10^{-4}$), a lot of computation time is spent which does not contribute to precipitate growth. Currently, schemes where f_V^M is significantly reduced by slightly adapting the AKMC algorithm while keeping the correct physical time evolution of the system are under investigation. Such a scheme in combination with parallelisation of the code would speed up our simulations by an order of magnitude. Other schemes that are under consideration, specifically in the pure coarsening stage, are first passage acceleration methods [55].

Despite the limitations of the AKMC simulations, good qualitative agreement with experiments was found. We stress the fact that the combination of a ternary many-body interatomic potential and the ANN based AKMC is able to produce very accurate time dependent simulations. Due to the many-body character of our potential, the results are directly transferrable to MD or other schemes that can account for relaxations. This is impossible to accomplish for the case of simple pair bonding potentials or DFT parameterizations used in other works [21, 22, 41, 49, 53].

5. Summary and conclusions

A many-body interatomic potential for the ternary Fe-Cu-Ni alloy was developed for the purpose of modelling radiation damage in reactor pressure vessel steels. For this purpose, we used previously developed, state-of-the-art Fe-Cu and Fe-Ni potentials, expressedly aimed at modelling radiation damage. The Cu-Ni cross potential was fitted to the experimental phase diagram and the DFT calculated interaction energies of Cu-Ni defect complexes in the bcc Fe matrix, so that a truly ternary potential was obtained.

The potential was validated by computing the Cu-Ni phase diagram, the interactions between Cu precipitates and Ni, and a simulated thermal annealing of the Fe-1.13Cu and Fe-1.13Cu-1.36Ni alloys at 823 K. The obtained phase diagram was found to be in reasonable agreement with the experimental one. The static calculations revealed a strong attraction between Ni and a Cu precipitate surface, which is consistent with experimental observations. In the thermal annealing simulations good qualitative agreement with experiments was established. The effects of the addition of Ni on average precipitate size and density showed similar trends as observed in experiments, notably increased density and reduced size, as a consequence of Ni enhancing Cu precipitate nucleation. In agreement with atom-probe

studies, Cu precipitates were found to be enriched by Ni on the precipitate surface. The latter effect was determined to be the consequence of the explusion of Ni from inside fully grown precipitates, rather than of transport of Ni atoms from the matrix to the surface of the precipitate. Quantitative comparison with experiments, however, could not be established, due to the inherent limitations of the used simulation techniques.

To conclude, we emphasize that, to the best of our knowledge, our Fe-Cu-Ni potential represents the first example of a ternary many-body potential developed to study radiation damage. Due to the many-body character of the potential, results obtained by different atomistic techniques are easily transferable, in contrast to the models currently available in the literature.

Appendix A: Parameterization of the cross potentials

The knots and fitting coefficients used in the cubic spline expansion (3) describing the mixed pair interactions are given in Table A1 for the Fe-Cu, Fe-Ni and Cu-Ni systems. The potentials used to describe the pure species, Fe, Cu, Ni, are given in the works by Mendelev *et al.* [25], Mishin *et al.* [26] and Voter and Chen [27], respectively. As mentioned in Section 2 all pure potentials must be transformed to the effective potential gauge to be compatible with the cross potentials derived here. With the superscript 'eff' denoting the pure potential functions, the needed transformation $\hat{T}$ is,

$$\hat{T}: \begin{cases} V^{\text{eff}}(r) = V(r) - 2Cj(r) \\ j^{\text{eff}}(r) = Sj(r) \\ F^{\text{eff}}(r) = F(r/S) + C/Sr \end{cases}, \qquad (C.1)$$

where *C* and *S* are constants given in Table A2. Tabulations of all the binary potentials can be found on-line following the link: http://www.ctcms.nist.gov/potentials/.

References

[1] J. P. Massoud, S. Bugat, J. L. Boutard, D. Lidbury, S. Van Dyck, F. Sevini, "Prediction of irradiation damage effects on reactor components (PERFECT)", in: "FISA 2006 EU Research and Training in Reactor Systems", G. Van Goethem, P. Manolatos, M. Hugon, V. Bhatnagar, S. Casalta and M. Deffrennes Eds., Directorare-General for Research, Euratom (Luxembourg, 2006).

[2] P. Pareige, J.C. Van Duysen and P. Auger, Appl. Surf. Sci. 67 (1993) p. 342.

[3] P. Pareige and M.K. Miller, Appl. Surf. Sci. 94/95 (1996) p. 370.

[4] M.K. Miller and K.F. Russell, J. Nucl. Mater. 371 (2007) p. 145.

[5] J. Kameda and A.J. Bevolo, Acta Metall. 37 (1989) p. 3283.

[6] Y. Nishiyama, K. Onizawa and M. Suzuki, J. ASTM Intl. 4 (2007) p. 83.

[7] U. Potapovs and J.R. Hawthorne, Nucl. Appl. 1 (1969) p. 27.

[8] G. Odette, Scr. Metall. 17 (1983) p. 1183.

[9] W. Phythian, C. English, J. Nucl. Mater. 205 (1993) p. 162.

[10] P. Auger, P. Pareige, A. Akamatsu, D. Blavette, J. Nucl. Mater. 225 (1995) p. 225.

[11] J.T. Buswell, W.J. Phytian, R.J. McElroy, S. Dumbill, P.H.N. Ray, J. Mace and R.N. Sinclair, J. Nucl. Mater. 225 (1995) p. 196.

[12] C. English, W. Phythian, R. McElroy, Mater. Res. Soc. Symp. Proc., vol. 439, MRS, Pittsburg, Pennsylvania, 1997, p. 471.

[13] G.R. Odette and G.E. Lucas, JOM 53 (2001) p. 18.

[14] Y. Nagai, Z. Tang, M. Hassegawa, T. Kanai, M. Saneyasu, Phys. Rev. B 63 (2001) p. 134110.

[15] K. Morita, S. Ishino, T. Tobita, Y. Chimi, N. Ishikawa, A. Iwase, J. Nucl. Mater. 304 (2002) p. 153.

[16] R. Chaouadi, R. Gérard, J. Nucl. Mater. 345 (2005) p. 65.

[17] C.L. Liu, G.R. Odette, B.D. Wirth and G.E. Lucas, Mater. Sci. Eng. A 238 (1997) p. 202.

[18] G.R. Odette and B.D. Wirth, J. Nucl. Mater. 251 (1997) p. 157.

[19] M.W. Finnis and J.E. Sinclair, Phil. Mag. A 50 (1984) p. 45.

[20] S.M. Foiles, M.I. Baskes and M.S. Daw, Phys. Rev. B 33 (1986) p. 7983.

[21] E. Vincent, C.S. Becquart and C. Domain, J. Nucl. Mater. 351 (2006) p. 88.

[22] E. Vincent, C.S. Becquart and C. Domain, Nucl. Instr. and Meth. B 255 (2007) p. 78.

[23] "Predicting Radiation-Induced Transition Temperature Shift in Reactor Vessel Materials, E706 (IIF)", ASTM International, E 900 - 02, 2007.

[24] M.S. Daw and M.I. Baskes, Phys. Rev. B 29 (1984) p. 6443.

[25] M.I. Mendelev, A. Han, D.J. Srolovitz, G.J. Ackland, D.Y. Sun and M. Asta, Phil. Mag. A 83 (2003) p. 3977.

[26] Y. Mishin, M.J. Mehl, D.A. Papaconstantopoulos, A.F. Voter, J.D. Kress, Phys. Rev. B 63 (2001) p. 224106.

[27] A.F. Voter and S.P. Chen, Mater. Res. Soc. Symp. Proc. 82 (1987) p. 175.

[28] F. Ercolessi, M. Parrinello and E. Tosatti, Phil. Mag. A 58 (1988) p. 213.

[29] R.A. Johnson and D.J. Oh, J. Mater. Res. 4 (1989) p. 1195.

[30] R.C. Pasianot and L. Malerba, J. Nucl. Mater. 360 (2007) p. 118.

[31] G. Bonny, R.C. Pasianot and L. Malerba, Model. Simul. Mater. Sci. Eng. 17 (2009) p. 025010.

[32] L. Malerba, M.-C. Marinica, N. Anento, C. Björkas, H. Nguyen, C. Domain, F. Djurabekova, P. Olsson, K. Nordlund, A. Serra, D. Terentyev, F. Willaime and C.S. Becquart, "Comparison of empirical interatomic potentials for iron applied to radiation damage studies", submitted to J. Nucl. Mater. (2009).

[33] C. Domain and G. Monnet, Phys. Rev. Lett. 95 (2005) p. 215506.

[34] G. Bonny, R.C. Pasianot and L. Malerba, "Fitting interatomic potentials consistent with thermodynamics: Fe, Cu, Ni and their alloys", submitted to Philos. Mag. (2009).

[35] S. Srikanth and K.T. Jacob, Mater. Sci. Technol. 5 (1989) p. 427.

[36] R.C. Sharma, Trans. Indian Inst. Met. 35 (1982) p. 372.

[37] S. Mey, Z. Metallkde. 78 (1987) p. 502.

[38] S. Mey, CALPHAD 16 (1992) p. 255.

[39] W.M. Young and E. W. Elcock, Proc. Phys. Soc. London 89 (1966) p. 735.

[40] F.G. Djurabekova, R. Domingos, G. Cerchiara, N. Castin, E. Vincent and L. Malerba, Nucl. Instr. and Meth. B 255 (2007) p. 8.

[41] H.C. Kang and W.H. Weinberg, J. Chem. Phys. 90 (1989) p. 2824.

[42] Y. Le Bouar and F. Soisson, Phys. Rev. B 65 (2002) p. 094103.

[43] N. Castin and L. Malerba, "Prediction of point defect migration energy barriers in alloys using artificial intelligence for atomistic kinetic Monte Carlo applications", accepted in Nucl. Instr. and Meth. (2009).

16

[44] G. Henkelman, G. Jóhannesson and H. Jónsson, "Methods for Finding Saddle Points and Minimum Energy Paths", Progress on Theoretical Chemistry and Physic, Ed. S.D. Schwartz (Kluwer Academic Publishers, 2000), p. 269.

[45] H. Jonsson, G. Mills, and K. W. Jacobsen, in Nudged Elastic Band Method for Finding Minimum Energy Paths of Transitions, Classical and Quantum Dynamics in Condensed Phase Simulations, Eds. B. J. Berne, G. Ciccotti, and D. F. Coker (World Scientific, Singapore, 1998).

[46] N. Castin, R.P. Domingos and L. Malerba, Intl. J. Comp. Intell. Sys. 1 (2008) p. 340.

[47] N. Castin and L. Malerba, "Artificial Intelligence regression of the vacancy migration energy to introduce relaxation effects in rigid lattice atomistic kinetic Monte Carlo simulations", submitted to J. Comp. Chem. (2009).

[48] J.T. Buswell, C.A. English, M.G. Hetherington, W.J. Phythian, G.D.W. Smith and G.M. Worrall, "An analysis of Small Clusters Formed in Thermally Aged and Irradiated FeCu and FeCuNi Model Alloys", Eds N.H. Packan *et al.*, Effects of Radiation on Materials: 14th International Symposium (Volume II), ASTM STP 1046, Philadelphia, 1990, p. 127.

[49] E. Vincent, C.S. Becquart, C.Pareige, P. Pareige, C. Domain, J. Nucl. Mater. 373 (2008) 387.

[50] S. Pizzini, K.J. Roberts and W.J. Phythian, Phil. Mag. Lett. 61 (1990) p. 223.

[51] P.J. Othen, M.L. Jenkins, G.D.W. Smith and W.J. Phythian, Phil. Mag. Lett. 64 (1991) p. 383.

[52] F. Maury, N. Lorenzelli, M.H. Mathon, C.H. de Novion and P. Lagarde, J. Phys.: Condens. Matter. 6 (1994) p. 569.

[53] F. Soisson and C.-C. Fu, Phys. Rev. B 76 (2007) p. 214102.

[54] A. Chatterjee and D.G. Vlachos, J. Comput.-Aided Mater. Des. 14 (2007) p. 253.

[55] T. Opplestrup, V.V. Bulatov, G.H. Gilmer, M.H. Kalos and B. Sadigh, Phys. Rev. Lett. 97 (2006) p. 230602.

Figure and table captions

Figure 1 – Comparison between mixing enthalpy obtained from our potential with Calphad parameterized ones based on experiments [35 ,38] for the Cu-Ni binary.

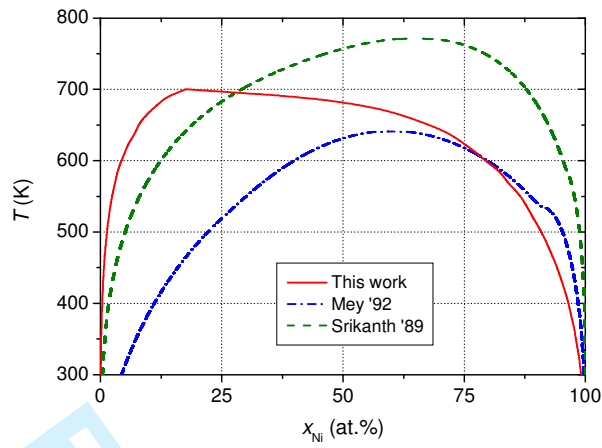Figure 2 – Comparison of the phase diagrams based on our potential and different Calphad parameterisations.
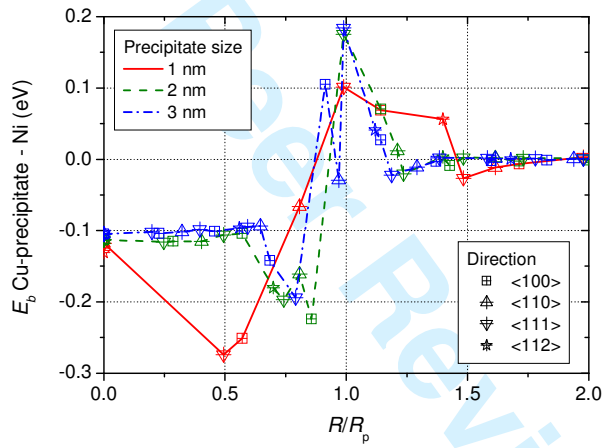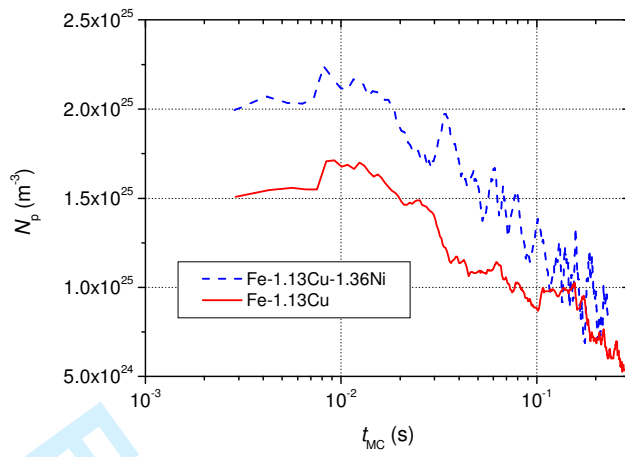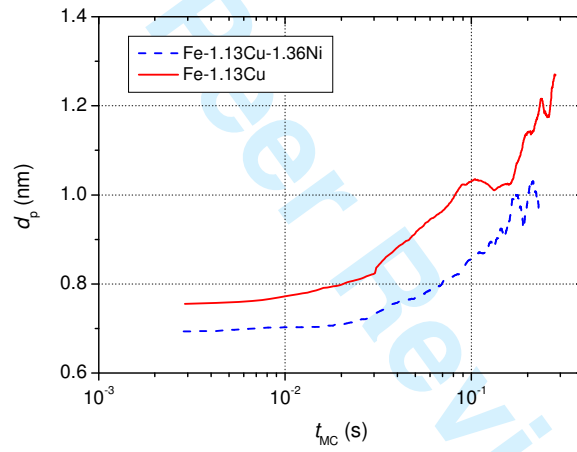
Figures and Tables

Fig. 1

Fig. 2

Fig. 3

Fig. 4

Fig. 5
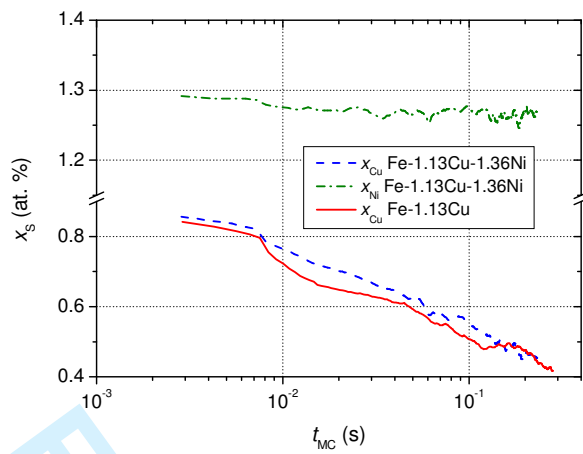
Fig. 6
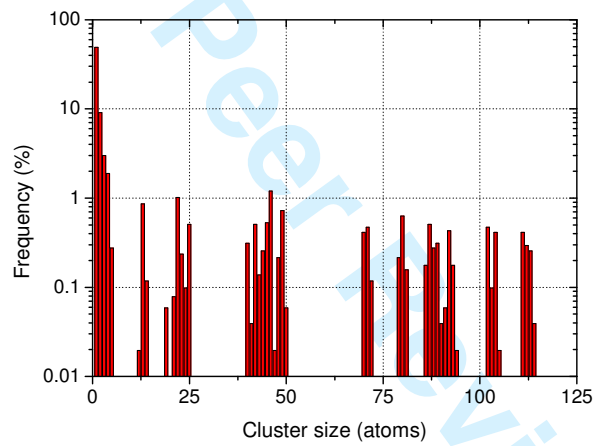
Fig. 7
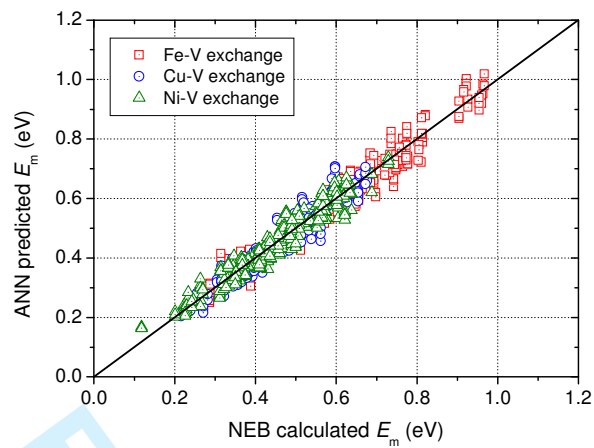
Fig. 8

Table 1

	This Work	DFT
E_b Cu-Ni (1nn)	0.01	0.02
E_b Cu-Ni (2nn)	0.07	-0.01
$E_b \langle 110 \rangle$ Cu-Ni	-0.37	-0.38

Table A1

	$V_{\text{Fe-Cu}}$		$V_{\text{Fe-Ni}}$		$V_{\text{Cu-Ni}}$	
i	r_i (Å)	a_i (eV/Å^3)	r_i (Å)	a_i (eV/Å^3)	r_i (Å)	a_i (eV/Å^3)
1	5.500000000	1.460151448E-03	5.500000000	1.01819400E-02	5.50000000	7.15210346E-03
2	5.257692308	-4.957562851E-02	5.000000000	-1.24535646E-01	5.18181818	-4.09422680E-02
3	5.015384615	6.998305005E-02	4.500000000	4.08902943E-01	4.86363636	2.69045453E-02
4	4.773076923	-3.874280553E-03	4.000000000	-7.37820671E-01	4.54545455	1.25068302E-02
5	4.530769231	-8.723411300E-03	3.500000000	5.91172697E-01	4.22727273	-2.23538031E-02
6	4.288461538	6.496879404E-02	3.000000000	4.84506404E-01	3.90909091	-4.05296894E-04
7	4.046153846	3.695651396E-03	2.500000000	1.24541131E+01	3.59090909	-2.13007867E-02
8	3.803846154	-5.082318050E-01	2.350000000	-2.50000000E+01	3.27272727	8.15583164E-02
9	3.561538462	-3.076315854E-01	2.200000000	5.00000000E+01	2.95454545	3.73700354E-01
10	3.319230769	2.117344729E+00			2.63636364	1.92883049E+00
11	3.076923077	-1.203932506E+00			2.31818182	8.25151398E+00
12	2.834615385	8.046491939E-03			2.30000000	-1.00000000E+01
13	2.592307692	2.703349799E+00			1.90000000	1.00000000E+02
14	2.350000000	4.000000000E+01				

Table A2

Species	C	S
Fe	0.116093429	0.0380008812
Cu	-0.00195739344	0.998555148
Ni	-24.3575774	2.92527845

106x83mm (600 x 600 DPI)

107x83mm (72 x 72 DPI)

108x83mm (72 x 72 DPI)
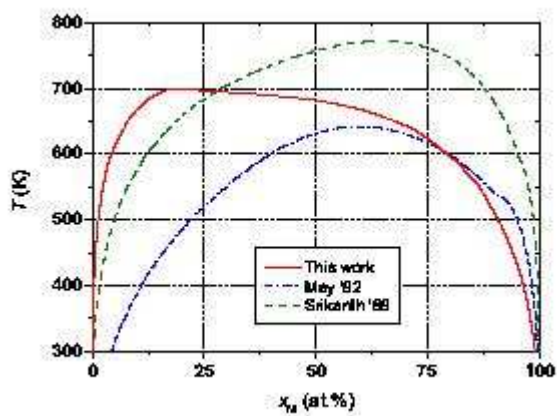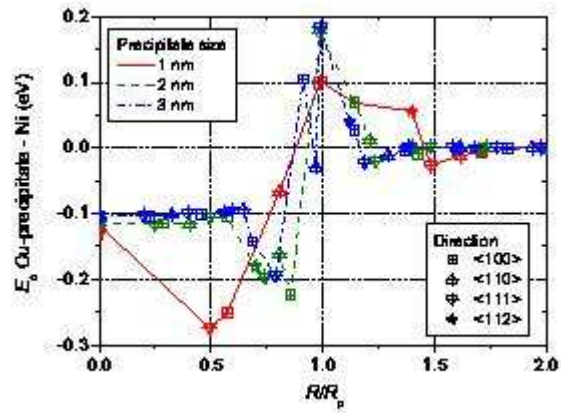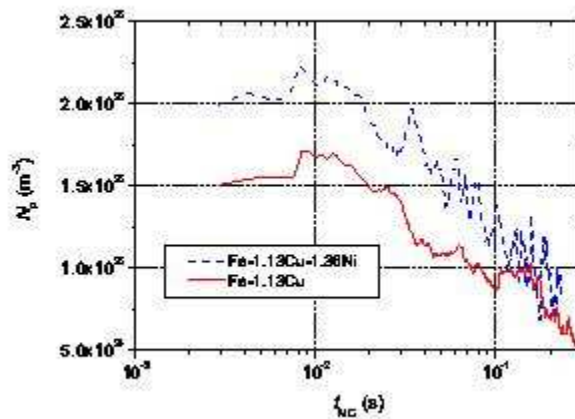
112x84mm (72 x 72 DPI)

104x83mm (72 x 72 DPI)

105x83mm (72 x 72 DPI)

1
2
3
4
5
6
7
8
9
10
11
12
13
14
15
16
17
18
19
20
21
22
23
24
25
26
27
28
29
30
31
32
33
34
35
36
37
38
39
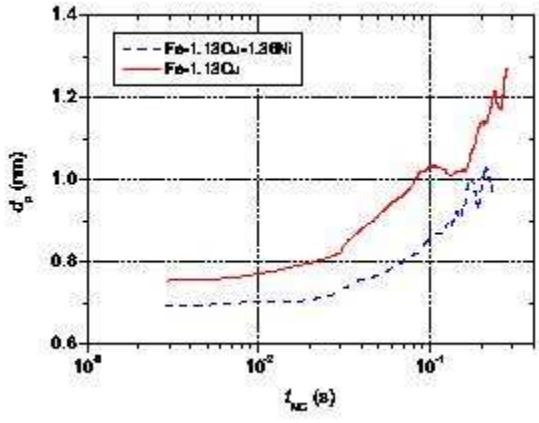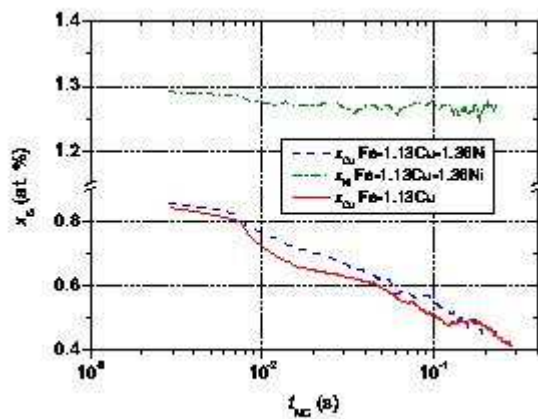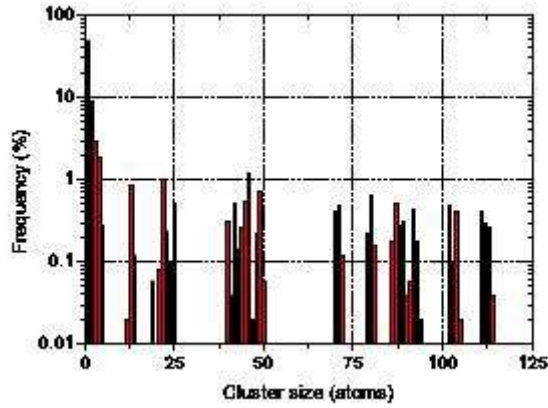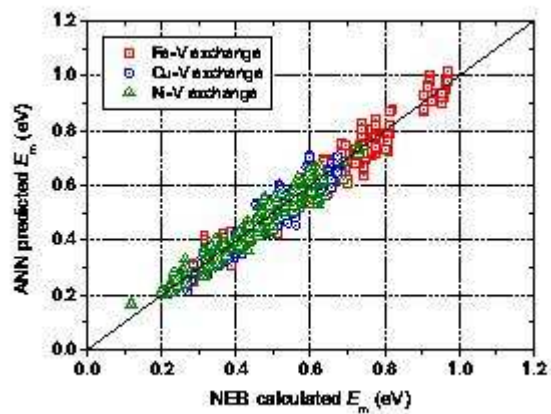40
41
42
43
44
45
46
47
48
49
50
51
52
53
54
55
56
57
58
59
60

106x82mm (72 x 72 DPI)

106x83mm (72 x 72 DPI)